Ultrafast Science
A SCIENCE PARTNER JOURNAL

RESEARCH ARTICLE

Strong Field Ionization Dynamics Resolved by Two-Color Elliptical Phase-of-Phase Spectroscopy

Wuwei Jin[1,2†], Tao Jiang[3,4†], Jinlei Liu[3,4*], Sizuo Luo[1,2*], Dianxiang Ren[1,2], Xiaokai Li[1,2], Chuncheng Wang[1,2], Yue Lang[3,4], Xiaowei Wang[3,4], Jing Zhao[3,4], Zengxiu Zhao[3,4*], and Dajun Ding[1,2*]

[1]Institute of Atomic and Molecular Physics, Jilin University, Changchun 130012, People's Republic of China. [2]Jilin Provincial Key Laboratory of Applied Atomic and Molecular Spectroscopy, Jilin University, Changchun 130012, People's Republic of China. [3]Department of Physics, National University of Defense Technology, Changsha 410073, People's Republic of China. [4]Hunan Key Laboratory of Extreme Matter and Applications, National University of Defense Technology, Changsha 410073, People's Republic of China.

*Address correspondence to: liujinlei@nudt.edu.cn (J.L.); luosz@jlu.edu.cn (S.L.); zhaozengxiu@nudt.edu.cn (Z.Z.); dajund@jlu.edu.cn (D.D.)
†These authors contributed equally to this work.

Citation: Jin W, Jiang T, Liu J, Luo S, Ren D, Li X, Wang C, Lang Y, Wang X, Zhao J, et al. Strong Field Ionization Dynamics Resolved by Two-Color Elliptical Phase-of-Phase Spectroscopy. *Ultrafast Sci.* 2024;4:Article 0066. https://doi.org/10.34133/ultrafastscience.0066

Submitted 3 June 2024
Accepted 16 June 2024
Published 5 September 2024

We investigate the strong field ionization of argon using counter-rotating 2-color dual-elliptical phase-of-phase spectroscopy. We perform a multidimensional control experiment over the 2-color dual-elliptical laser field to modulate the photoelectron momentum spectra generated under strong fields. Incorporating the classical trajectory Monte Carlo calculation, we study the behavior of the relative phase contrast and the phase of phase and clarify how the enhancement of temporal precision in angular resolution measurements is achieved when the relative phase corresponds to the frequency of 3ω. Our results uncover the potential for using quantitatively controlled 2-color elliptical fields to realize precise probes of the attosecond ionization and scattering dynamics.

Introduction

Strong field ionization and excitation trigger a broad range of ultrafast phenomena in the interaction of atoms, molecules, and solids with strong laser pulses, such as high-order harmonics generation, below-threshold harmonics, air lasing, and terahertz (THz) wave emission, which has laid the foundation for strong field physics and attosecond science [1–6]. Of particular interest is whether tunnelling takes time and how it can be measured. The advancement of laser manipulating and shaping technology enables the precise control of strong field electron dynamics on a subcycle time scale, which helps to resolve this critical issue. Two-color fields, which are the coherent overlap of the strong driving laser fields and its second-harmonic field acting as a perturbation, provide an easy-to-implement method to shape the tunnelling electron wavepacket and control the coherent radiation [7–10]. Circularly or elliptically polarized fields provide a time-resolved approach to access the quantum dynamics through mapping subcycle tunnelling bursts to different emission angles, which is termed as an attoclock [11–14]. Incorporating the advantages of 2-color fields and circularly polarized fields, 2-color circularly polarized laser fields offer additional control to the attoclock measurement of tunnelling dynamics and the generation of circularly polarized high harmonics and THz wave [15–20].

To retrieve the dynamic information from the multi-parameter-dependent photoelectron spectroscopy, the powerful phase-of-phase (POP) technique has been proposed to reveal the structural information of atoms and molecules by analyzing the dependence of photoelectron momentum distribution as a function of the relative phase ϕ_{RP}, $Y(\mathbf{p},\phi_{RP}) \simeq Y_0(\mathbf{p}) + \Delta Y_1(\mathbf{p}) \cos(\phi_{RP} + \Phi_{POP}(\mathbf{p}))$ [21,22]. The momentum-resolved photoemission signal is Fourier transformed with respect to the relative phase, and 2 key parameters are obtained: (a) the relative phase contrast (RPC), ΔY_1, which is the magnitude of the Fourier transform and gives the strength of the photoelectron yield modulation, and (b) the POP, Φ_{POP}, which is the phase of the Fourier transform and gives information about signal modulation to the relative phase. It has been shown that POP spectroscopy can be used to extract the laser-coherent part of the photoelectron spectra taken under complex target conditions such as nanodroplets [23], or probe the nonstationary tunnelling dynamics by manipulating a rapidly changing potential barrier [24]. Recently, POP spectroscopy, which employs a strong elliptically polarized laser pulse combined with a perturbative linearly polarized second-harmonic field to modulate the tunnelling current generated by the strong elliptically polarized laser in attoclock configurations, has been utilized to accurately determine tunnelling ionization times with a precision of a few attoseconds. However, as the electron energy increases, the most probable emission angle for tunnelling ionization shifts to earlier ionization times, contradicting

predictions made by classical trajectory models [25]. In another work, counter-rotating or co-rotating 2-color circularly polarized fields are employed, where difficulties arise from the precise manipulating of the ellipticity of the strong laser fields [26].

In this manuscript, we demonstrate POP attoclock spectroscopy using 2-color dual-elliptically polarized laser fields. We experimentally measure the photoelectron momentum spectra of argon in counter-rotating 2-color strong fields. The experimental RPC and POP spectra agree well with the calculation results using the classical trajectory Monte Carlo (CTMC) method [8]. The POP range in using counter-rotating elliptically polarized fields is triple the POP range using co-rotating elliptically polarized fields, realizing an enhancement of temporal measurement resolution. The time delay extracted from POP spectra at the yield peak angle is determined to be close to zero within the experimental accuracy. POP attoclock spectroscopy using 2-color elliptically polarized laser fields is a promising approach to attosecond measurement of electron motion in atoms and molecules. Atomic units are used unless stated otherwise.

Methods

The experimental setup [14,26] is depicted in the lower section of Fig. 1. The upper section illustrates the progression of the laser field along the optical path and the step-by-step realization of multidimensional control. Initially, linearly polarized femtosecond laser pulses (35 fs, 800 nm, 1 kHz, 4 mJ) are produced using a chirped pulse amplified Ti: sapphire system. In the first outlined area, the second-harmonic (400 nm) pulse is introduced by a 0.5-mm β barium borate (β-BBO) crystal and it collinearly propagates with the fundamental pulse to keep the 2-color relative phase stable. A 5-mm calcite crystal offsets the time delay coarsely, specifically the 2-color relative phase (ϕ_{RP}), caused by the group velocity disparity between the 800-nm and 400-nm pulses. In the second outlined area, the precise control of the relative phase

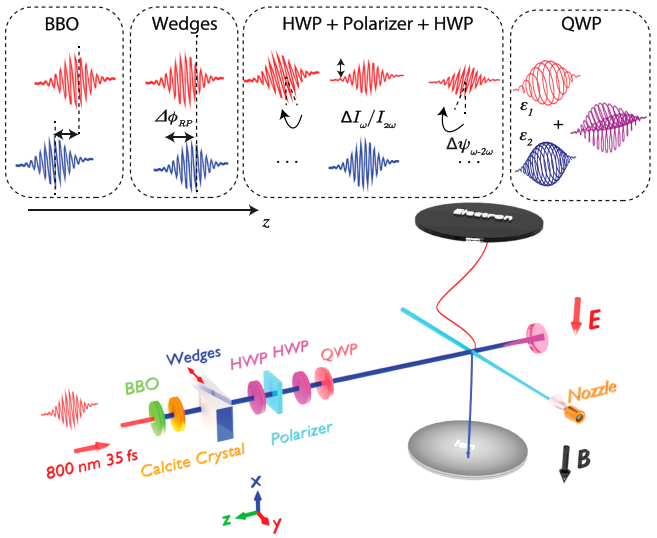

Fig. 1. Schematic diagram of the experimental setup. The laser propagates along the *z* axis and the polarization plane of 2-color pulses lies in the *x*-*y* plane. The upper diagram shows the transformation of the temporal waveform from linearly polarized laser pulses to the counter-rotating 2-color elliptically polarized pulses, of which the relative phase delay, the relative intensity ratio, and the ellipticities can be controlled. E and B represent the directions of the electric field and magnetic field, respectively.

(ϕ_{RP}) between the 2 pulses is achieved using a pair of fused silica wedges (40 mm length, 4 mm thickness) mounted on a translation stage. In the subsequent section, the intensity of the 800-nm laser pulse is modulated by a combination of a half-wave plate (HWP) and a linear polarizer. The intensity ratio $I_{2\omega}/I_\omega$ is regulated by rotating the 800-nm laser only to alter its transmission through the linear polarizer. Following this, another HWP adjusts the polarization angle between the 2 laser pulses ($\Delta\psi_{\omega-2\omega}$). In the last segment, the dual quarter-wave plate (QWP) simultaneously transforms the 2-color laser pulses from linear polarized to circularly or elliptically polarized, with the QWP angle fine-tuning the ellipticities (ε) of both pulses. This comprehensive setup enables versatile manipulation of the relative phase delay, intensity ratio, and ellipticities of the 2-color pulses. The relative phase between 2 color laser pulses is calibrated by the measured ionization yields and photoelectron spectra when we scanned over the pulses and compared them with theory. The focused 2-color laser pulses, directed onto a supersonic argon gas jet through a concave mirror ($f = 75$ mm), facilitate the measurement of photoelectron momentum spectra using cold-target recoil-ion momentum spectroscopy (COLTRIMS) [27].

To compare with the measurements, we calculate the photoelectron spectra of the argon subjected to the 2-color elliptically polarized laser field using the CTMC method [8]. The synthesized electric field can be expressed as

$$E(t) = f(t)\{\left[E_\omega \cos(\omega t) + E_{2\omega}\sin\left(2\omega t + \phi_{RP}\right)\right]\hat{x} + \left[\varepsilon_1 E_\omega \sin(\omega t) + \varepsilon_2 E_{2\omega}\cos\left(2\omega t + \phi_{RP}\right)\right]\hat{y}\} \quad (1)$$

where ε_1 and ε_2 are the ellipticities of the fundamental wave 800 nm and the second-harmonic wave 400 nm, respectively. The stronger fundamental wave is used to trigger the dynamical subcycle tunnelling bursts, and the weaker counter-rotating second harmonic serves to perturb the potential barrier uniformly and to probe the time-dependent tunnelling dynamics by adjusting the 2-color relative phase (ϕ_{RP}). The peak intensities of the fundamental field and the second-harmonic field are chosen as $I_\omega = 2\times10^{14}$ W/cm^2 and $I_{2\omega} = 2\times10^{13}$ W/cm^2, respectively. $f(t)$ is the laser envelope with pulse duration $\tau = 35$ fs, which is chosen as a sine-square function in the calculation.

In the CTMC calculation, electrons are assumed to tunnel out along the polarization axis at every instant t_0 with initial momentum distribution and ionization rate predicted by the Ammosov, Delone, and Krainov (ADK) tunnelling theory [28,29]. The initial longitudinal momentum (along the instantaneous laser polarization) is taken as zero, while the initial transverse momenta $p_\perp^i$ (perpendicular to the instantaneous laser polarization) have a Gaussian distribution with a half-width of $\sigma_\perp = \sqrt{|E(t_0)|/\sqrt{2I_p}}$, where I_p is the ionization potential of argon. The ionization moment and the initial lateral momentum are sampled as 2 coordinates of a uniform random variable in the parameter space $[0,\tau]$ and $[-3\sigma_\perp, 3\sigma_\perp]$. In addition, the directions of the initial transverse momenta are assumed uniformly pointed at angles of $[0,2\pi]$ [8,12]. Integrating Newton's equation under the combined field of the laser field and the Coulomb potential, the position $\mathbf{r}$ and the momentum $\mathbf{q}$ of the electron at the end of the laser pulse are obtained, while the angular momentum $\mathbf{M} = \mathbf{r}\times\mathbf{q}$ and the Laplace–Runge–Lenz vector $\mathbf{A}_{LRL} = [\mathbf{q}\times\mathbf{M}] - \frac{\mathbf{r}}{r}$ can be identified [30]. From the energy

conservation law $\frac{p^2}{2} = \frac{q^2}{2} - \frac{1}{r}$, the magnitude of the asymptotic momentum p is determined and the asymptotic momentum $\mathbf{p}$ is calculated using a simple formula [31,32].

Results and Discussion

Figure 2A and B shows the experimental and the calculated photoelectron momentum spectra of Ar atoms in the counter-rotating 2-color elliptically polarized laser field with the measured parameters of $\varepsilon_\omega = 0.89$, $I_\omega = 2 \times 10^{14}$ W/cm^2, $\varepsilon_{2\omega} = 0.68$, $I_{2\omega} = 2 \times 10^{13}$ W/cm^2, and $\phi_{RP} = 0.8\pi$. For the convenience of comparison, the yields of photoelectrons in both spectra are normalized. The observed "3-leaf clover" pattern in the momentum spectra verifies the threefold symmetry of the laser vector potential due to the near-circularly polarized 800-nm laser field [16,23]. The photoelectron yield attains a maximum near $2U_p$, where $U_p = E_\omega^2 / 4\omega^2$ is the ponderomotive energy. For the intensity uncertainty in experiments, the energy width of the experimental spectrum is larger than the calculated spectrum. In Fig. 2B and C, we compare the photoelectron momentum distribution at a relative phase of 0.8π under 2 different intensity ratios of $I_{2\omega}/I_\omega$, specifically 1:10 and 1:100. The results show that under weaker light intensity ratios, the 3-leaf clover structure degenerates into a bilobed structure.

Based on the measured and calculated photoelectron spectra with different relative phases (ϕ_{RP}), we perform the Fourier transform to extract the RPC (ΔY_1) and POP (Φ_{POP}) in Fig. 3. The POP spectra from measured and calculated results displayed in Fig. 3B and D agree well within [5 eV,15 eV], and the POP modulates within a range of 6π when photoelectron emission angle changes from 0 to 2π. Thus, the 3ω component shows up in the POP map, which arises in the counter-rotating 2-color configuration. The agreement indicates that the electrons are mainly emitted once every 0.89 fs, which is dominated by the threefold symmetry electric field with one laser cycle (2.67 fs) at 800 nm. The Fourier analysis of periodic oscillation signals in the full momenta space provides the ability for better temporal resolution, circumventing limitations imposed by angular resolution during conventional attoclock measurement. In contrast, Fig. 3F presents comparable POP spectra calculated under the same conditions, except for employing co-rotating 2-color laser pulses. Here, the POP modulates within a 2π range. Meanwhile, despite only 2-lobe momenta distribution being observed under lower laser intensity ratios (same condition used in Fig. 2C), the POP spectra still exhibit 3ω characteristics as shown in Fig. 3H, indicating that counter-rotating configuration is the primary factor driving the 3ω pattern. The 6π range of POP variation enables the resolving of ionization dynamics; particularly, the retrieval of tunnelling time by accuracy improved by a factor of 3.

The RPC spectra in Fig. 3A and C display 2 predominant emission angles when the electron's energy is below $2U_p$ in measured and calculated results, which is the same as co-rotating RPC spectra in Fig. 3E [24]. According to Eq. 1, the field magnitude takes maximum at $t = 0$ or $t = \pi$ regardless of the modulation with the relative phase. Hence, the momentum of the ejected electron is along 90° and 270° if it is purely driven by the laser field neglecting the influence of the Coulomb potential. However, the observed emission angles with yield peaks are identified as 73° and 253° by Gaussian fitting of the energy-integrated yields. The calculated yield peak from the RPC with the influence of Coulomb potential is in close agreement with the measured results, which are 73. 4° and 252. 6°. The difference of the fitted peak angles from 90° and 270° can be attributed to the effect of the Coulomb potential on the offset angle, commonly observed in elliptically polarized laser fields. The CTMC approach provides an effective way to separate the long-range Coulomb field and the corresponding effect; thus, it can determine the influence of tunnelling ionization delay [11,12,33,34]. In addition, the shape of the RPC spectra indicates that the Coulomb potential-induced distortion depends on the final momentum of the ejecting electron, which plays a important role in THz wave generation [7,8].

From the POP spectra in Fig. 3, we also identify a novel feature at high energy region ([15 eV,25 eV]) only in 6π cases: A peculiar, very sharp phase flip between direct ionization and scattering ionization has been observed. The phase flip shows clear angular dependence due to the combination of 2 elliptically polarized laser fields and gives approximately π phase jump when scattering becomes dominant. Previous theoretical studies have noted that some momentum-resolved Fourier components' phase lag sharply flips along certain momentum–space

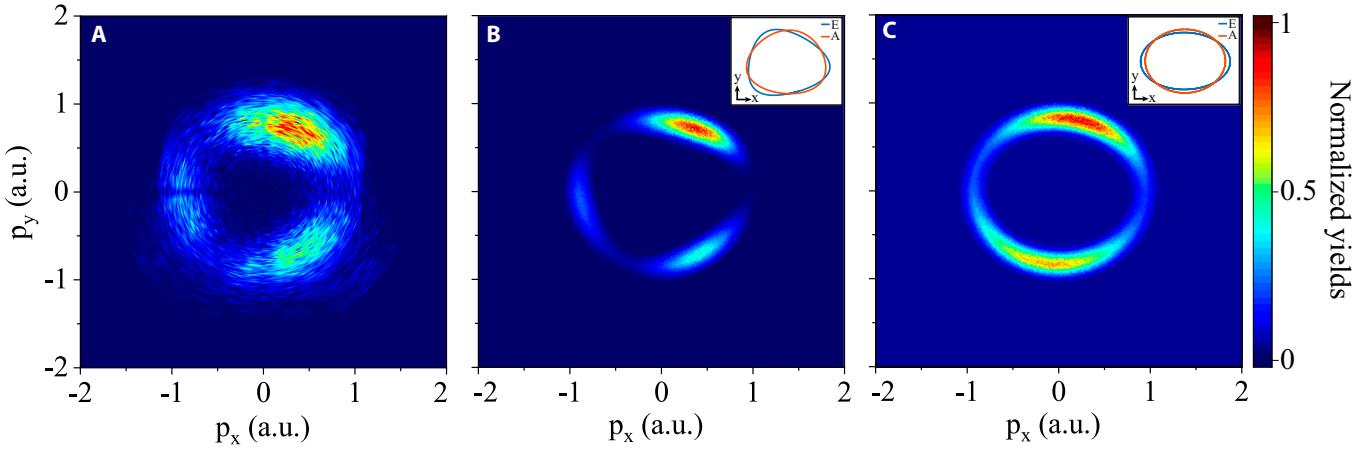

Fig. 2. (A) Experimentally measured photoelectron momentum distribution at the relative phase of 0.8π of Ar in the 2-color elliptically polarized fields combined with a strong 800-nm fundamental field ($\varepsilon_\omega = 0.89$, $I_\omega = 2 \times 10^{14}$ W/cm^2) and a weak counter-rotating second harmonic ($\varepsilon_{2\omega} = 0.68$, $I_{2\omega} = 2 \times 10^{13}$ W/cm^2). (B) Calculated photoelectron momentum distribution using CTMC under the same laser parameters. An inset figure displays the electric field of the 2-color field. (C) Calculated photoelectron momentum distribution with a counter-rotating second harmonic that is 10 times weaker ($I_{2\omega} = 2 \times 10^{12}$ W/cm^2). An inset figure also displays the electric field of the 2-color field.

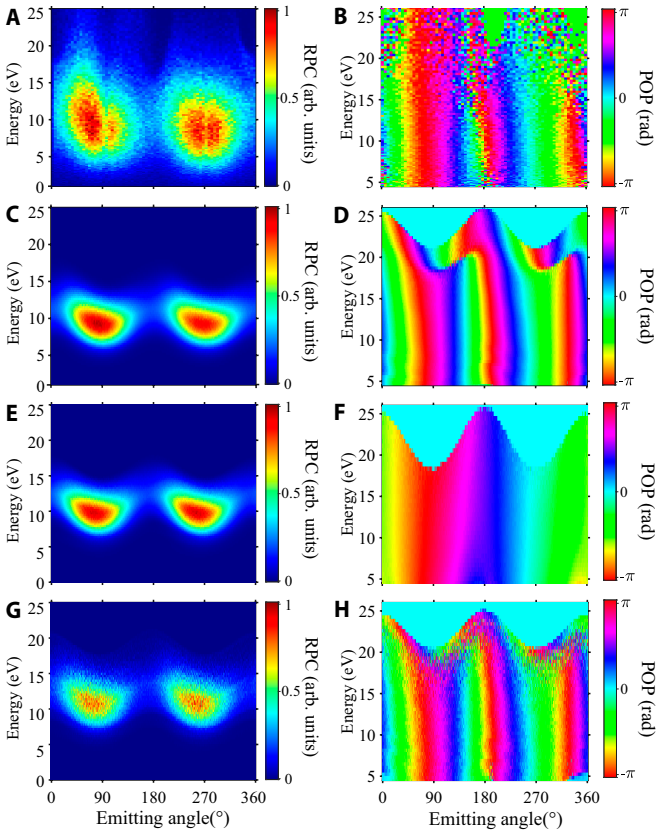

Fig. 3. (A) and (C) present both the measured and calculated RPC spectra, alongside the POP spectra in (B) and (D), derived from the photoelectron spectra at different ϕ_{RP} angles. These spectra were obtained under the same laser parameters as those detailed in Fig. 2, allowing for direct comparison. (E) and (F) display the spectra for the co-rotating case, also under the same laser conditions, serving as a comparative analysis. (G) and (H) display the spectra for cases with 10 times weaker laser intensity ratios and also serve as a comparative analysis.

curves [23]. These "flipping curves" are sensitive to the system's parameters and have been attributed to the scattering interactions between electrons and ions or neutral atoms [35]. However, for fast photoelectrons, where countings are low due to the significantly reduced ionization probability, these flipping curves may not be easily resolved due to the sparse number of events detected in the experiment. Meanwhile, the phase flip phenomenon is markedly pronounced in higher laser intensity ratios than in lower cases (compare Fig. 3D and H). The flip occurs when the electron energy surpasses the energy from direct tunnelling ionization, i.e. $\sim 2U_p$, at which energy the scattering starts to dominate [36]. This phenomenon is not observed in the co-rotating configuration, as shown in Fig. 3E and F, due to the significant suppression of scattering electrons in the high ellipticity laser field. We also observed weak signals at the high energy region during measurement, as evidenced in Fig. 3B, which shows a trend indicative of phase flipping. Therefore, the present experiment clearly demonstrates that higher laser intensity ratios enhance POP spectra resolution, facilitating the observation of phase flip phenomena that are sensitive to both laser parameters and electron scattering. This showcases the capability to distinguish and detect the attosecond dynamics of direct ionization and scattering processes.

Once the angle of the peak emission is determined from RPC, the major tunnelling event can be particularly ascribed.

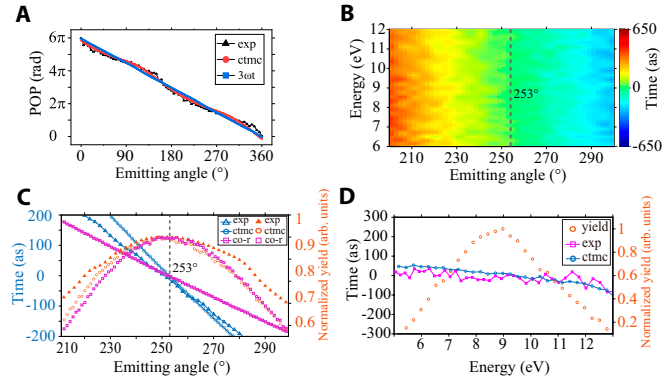

Fig. 4. (A) The cumulative POP as a function of emission angle is graphically represented. Black triangles mark the experimental data, red circles denote the theoretical predictions, and blue squares illustrate the $3\omega t$ curve employed for linear calibration. (B) The time-delay mapping was retrieved from the experimental POP spectra. The gray vertical dashed line represents the peak emission angle 253°. (C) The cross-sectional view of the time delay, as it relates to the electron emission angle, is presented for both the measured and calculated results (co-rotating with the same parameters), depicted by blue triangles and circles (purple square). Additionally, the energy-integrated electron yield is illustrated, which helps to determine the peak emission angle for both measured and calculated outcomes, represented by red triangles and circles, respectively. (D) Energy-resolved yield (red circles) and time delay for different energy along the emission angle of 253°. Experimental and calculated time delay for each energy are represented using purple squares and blue circles, respectively.

If the oscillation of the electron yield is in phase with the oscillation of the electric field strength at the instant of time, the tunnelling ionization time is determined. The time delay of the tunnelling ionization that imprints on the modulation of the spectra can be retrieved from the POP spectra for each emission momentum and angle [25] using

$$\tau(\mathbf{p}) = -\Phi_{\mathrm{POP}} / (2\omega). \tag{2}$$

According to the definition, time zero refers to the scenario where the Φ_{POP} change is zero. To more effectively illustrate the relationship between POP and emission angle, we have integrated the POP spectra over the energy range. Throughout a complete emission angle cycle, the POP experiences 3 phase changes across $[0, 2\pi]$. Figure 4A displays the total cumulative POP as a function of varying emission angles for both measured and calculated results. We apply a linear calibration curve using $3\omega t$. The variation from the linear dependence suggests that the attoclock's "hand" is not rotating uniformly, which can be ascribed to the effects of the weaker counter-rotating second-harmonic perturbation. In comparison to the ωt condition, the scenario with $3\omega t$ demonstrates a steeper slope, indicating the potential to triple the time-delay resolution for each unit of emission angle. Concentrating on the emission angle at the yield peak, we deduced the time delay using the POP spectra. The time-delay map, extracted from the experimental POP spectra near the yield peak at an emission angle of 253°, is presented in Fig. 4B. A gray vertical dashed line within the figure highlights this peak emission angle. Around the yield peak, the measured and calculated yield from the RPC across all energy are denoted by the red triangles and circles in Fig. 4C. The angle-dependent time delay, upon evaluation, is found to be near zero for both experimental and theoretical calculations, consistent with tunnelling time findings in prior studies [12,13,25]. Nevertheless, the contention regarding the absence of tunnelling time persists,

largely due to the resolution limitations in measuring time delay per unit of emission angle [6].

Further analysis has been conducted on the energy variation in relation to the emission angle, as depicted in Fig. 4D. This figure illustrates the distribution of the energy-resolved electron yield and the corresponding time delay at the peak emission angle. The electron yield, indicated by red circles, reveals that the most probable electron energy resulting from ionization at this peak emission angle is approximately 9 eV. Additionally, this analysis shows a distribution of tunnelling emission angles that varies with electron energy. Specifically, electrons with lower energies exhibit tunnelling angles greater than 253°, while those with higher energies have angles less than 253°. The measurement has been quantified and reproduced by the CTMC simulation, which rectifies the previous contradicts between experiments and classical trajectory simulation [25]. Our work not only showcases a tripling of angular resolution capabilities but also confirms that the experimental results are consistent with theoretical predictions. We note that the non-adiabatic effect in strong field tunnelling manifests in the tunnelling position variation, the initial tunnelling momentum distributions at the tunnel exit, and the ionization rate [37,38]. The non-adiabatic effect has a measurable influence in the traditional attoclock experiments where only the offset angle is used to retrieve the tunnelling time information [39,40]. However, the POP attoclock scheme, which measures the tunnelling time based on the correspondence between the RPC and the POP phase, overcomes the difficulties in previous attoclock measurements, which require the precise measurement of the driving laser fields and the photoelectron momentum distribution [25]. Furthermore, the corresponding Keldysh parameter γ is around 0.8 in our experiment; thus, the tunnelling picture is appropriate to describe the strong field ionization. So the influence of the non-adiabatic effect in tunnelling time measurement using POP attoclock is limited. The tunnelling time's precision in POP attoclock depends on the POP's accuracy in the Fourier transform. The counter-rotating POP attoclock has a 6π POP range, which is 3 times of co-rotating scheme. A higher POP resolution, defined as $R = 1/\Delta\Phi_{POP}$, can be obtained in the counter-rotating POP attoclock.

Conclusion

In conclusion, we present the 2-color counter-rotating elliptical POP spectroscopy as a novel approach to investigate the dynamics of strong ionization. An experimental multidimensional control on 2-color laser fields is performed to obtain the modulated electron momentum spectra. Combined with the CTMC method, we calculate the POP and RPC spectra and retrieve tunnelling time around the RPC peak. Our findings reveal that the photoelectron yield, oscillating with relative phase at a frequency of 3ω, significantly enhances angular resolution capabilities. This system notably improves the efficiency of investigating high-energy electron scattering signals at higher laser intensity ratios. Additionally, we observed the clear correlations between the measured time delay with the emission angles and the electron energies, which underscore the advantages of the accuracy of the POP spectrum retrieved from the 3ω component. The 2-color elliptical POP spectroscopy is a promising method to enhance attosecond temporal resolution in the in situ measurement of a strong laser field.

Acknowledgments

Funding: This work is supported by the National Basic Research Program of China (grant no. 2019YFA0307700), the NSF of China (grant nos.12134005, 12234020, 12274461, and 11974426), the NSF of Hunan Province (grant no. 2023JJ10049), and the Foundation of National University of Defense Technology (grant no. ZK22-31).

Author contributions: S.L., J.L., Z.Z., and D.D. conceived and supervised the project. W.J, D.R., X.L., C.C, and S.L. performed the experiments, T.J., J.L., Y.L., X.W., and J.Z. carried out the simulations. W.J, T.J., J.L., S.L., Z.Z., and D.D. wrote the manuscript. All authors discussed the results and commented on the manuscript.

Competing interests: The authors declare that they have no competing interests.

Data Availability

The data that support the plots within this paper will be available from the corresponding authors upon reasonable request.

References

1. Corkum PB. Plasma perspective on strong field multiphoton ionization. *Phys Rev Lett*. 1993;71(13):1994–1997.
2. Ghimire S, DiChiara AD, Sistrunk E, Agostini P, DiMauro LF, Reis DA. Observation of high-order harmonic generation in a bulk crystal. *Nat Phys*. 2011;7:138–141.
3. Yun H, Mun JH, Hwang SI, Park SB, Ivanov IA, Nam CH, Kim KT. Coherent extreme-ultraviolet emission generated through frustrated tunnelling ionization. *Nat Photonics*. 2018;12:620–624.
4. Lei H, Yao J, Zhao J, Xie H, Zhang F, Zhang H, Zhang N, Li G, Zhang Q, Wang X, et al. Ultraviolet supercontinuum generation driven by ionic coherence in a strong laser field. *Nat Commun*. 2022;13(1):4080.
5. Xie X, Dai J, Zhang X-C. Coherent control of THz wave generation in ambient air. *Phys Rev Lett*. 2006;96(7):Article 075005.
6. Quan W, Serov VV, Wei M, Zhao M, Zhou Y, Wang Y, Lai X, Kheifets AS, Liu X. Attosecond molecular angular streaking with all-ionic fragments detection. *Phys Rev Lett*. 2019;123(22):223204.
7. Zhang D, Lü Z, Meng C, Du X, Zhou Z, Zhao Z, Yuan J. Synchronizing terahertz wave generation with attosecond bursts. *Phys Rev Lett*. 2012;109(24):243002.
8. Liu J, Chen W, Zhang B, Zhao J, Wu J, Yuan J, Zhao Z. Trajectory-based analysis of low-energy electrons and photocurrents generated in strong-field ionization. *Phys Rev A*. 2014;90:Article 063420.
9. Henkel J, Lein M. Analysis of electron trajectories with two-color strong-field ionization. *Phys Rev A*. 2015;92(1):Article 013422.
10. Huang Y, Zhao J, Shu Z, Zhu Y, Liu J, Dong W, Wang X, Lü Z, Zhang D, Yuan J, et al. Ultrafast hole deformation revealed by molecular Attosecond interferometry. *Ultraf Sci*. 2021;2021:1–12.
11. Eckle P, Pfeiffer A, Cirelli C, Staudte A, Dorner R, Muller H, Buttiker M, Keller U. Attosecond ionization and tunneling delay time measurements in helium. *Science*. 2008;322(5907):1525–1529.
12. Liu J, Fu Y, Chen W, Lü Z, Zhao J, Yuan J, Zhao Z. Offset angles of photocurrents generated in few-cycle circularly polarized laser fields. *J Phys B At Mol Phys*. 2017;50(5):Article 055602.

13. Sainadh US, Xu H, Wang X, Atia-Tul-Noor A, Wallace WC, Douguet N, Bray A, Ivanov I, Bartschat K, Kheifets A, et al. Attosecond angular streaking and tunnelling time in atomic hydrogen. *Nature*. 2019;568(7750):75–77.
14. Luo S, Liu J, Li X, Zhang D, Yu X, Ren D, Li M, Yang Y, Wang Z, Ma P, et al. Revealing molecular strong field autoionization dynamics. *Phys Rev Lett*. 2021;126(10):103202.
15. Vvedenskii NV, Korytin AI, Kostin VA, Murzanev AA, Silaev AA, Stepanov AN. Two-color laser-plasma generation of terahertz radiation using a frequency-tunable half harmonic of a femtosecond pulse. *Phys Rev Lett*. 2014;112(5):Article 055004.
16. Mancuso CA, Hickstein DD, Grychtol P, Knut R, Kfir O, Tong X-M, Dollar F, Zusin D, Gopalakrishnan M, Gentry C, et al. Strong-field ionization with two-color circularly polarized laser fields. *Phys Rev A*. 2015;91(3):Article 031402.
17. Meng C, Chen W, Wang X, Lü Z, Huang Y, Liu J, Zhang D, Zhao Z, Yuan J. Enhancement of terahertz radiation by using circularly polarized two-color laser fields. *Appl Phys Lett*. 2016;109(3):131105.
18. Ge P, Han M, Deng Y, Gong Q, Liu Y. Universal description of the Attoclock with two-color Corotating circular fields. *Phys Rev Lett*. 2019;122(1):Article 013201.
19. Eicke N, Lein M. Attoclock with counter-rotating bicircular laser fields. *Phys Rev A*. 2019;99(3):Article 031402.
20. Guo Z, Ge P, Fang Y, Dou Y, Yu X, Wang J, Gong Q, Liu Y. Probing molecular frame Wigner time delay and electron wavepacket phase structure of CO molecule. *Ultraf Sci*. 2022;2022(6):1–10.
21. Skruszewicz S, Tiggesbäumker J, Meiwes-Broer K-H, Arbeiter M, Fennel T, Bauer D. Two-color strong-field photoelectron spectroscopy and the phase of the phase. *Phys Rev Lett*. 2015;115(4):Article 043001.
22. Almajid MA, Zabel M, Skruszewicz S, Tiggesbäumker J, Bauer D. Two-color phase-of-the-phase spectroscopy in the multiphoton regime. *J Phys B At Mol Phys*. 2017;50(19): Article 194001.
23. Tulsky VA, Almajid MA, Bauer D. Two-color phase-of-the-phase spectroscopy with circularly polarized laser pulses. *Phys Rev A*. 2018;98:Article 053433.
24. Han M, Ge P, Wang J, Guo Z, Fang Y, Ma X, Yu X, Deng Y, Wörner HJ, Gong Q, et al. Complete characterization of sub-coulomb-barrier tunnelling with phase-of-phase attoclock. *Nat Photonics*. 2021;15(10):765–771.
25. Yu M, Liu K, Li M, Yan J, Cao C, Tan J, Liang J, Guo K, Cao W, Lan P, et al. Full experimental determination of tunneling time with attosecond-scale streaking method. *Light Sci Appli*. 2022;11(1):215.
26. Wang C, Li X, Xiao X-R, Yang Y, Luo S, Yu X, Xu X, Peng L-Y, Gong Q, Ding D. Accurate in situ measurement of ellipticity based on subcycle ionization dynamics. *Phys Rev Lett*. 2019;122(1):Article 013203.
27. Ullrich J, Moshammer R, Dorn A, Dörner R, Schmidt LPH, Schmidt-Böcking H. Recoil-ion and electron momentum spectroscopy: Reaction-microscopes. *Rep Prog Phys*. 2003;66(9):1463.
28. Ammosov MV, Delone NB, Krainov VP. Tunnel ionization of complex atoms and atomic ions in electromagnetic field. *High Intens Laser Process*. 1986;64:138–141.
29. Delone NB, Krainov VP. Energy and angular electron spectra for the tunnel ionization of atoms by strong low-frequency radiation. *J Opt Soc Am B*. 1991;8(6):1207.
30. Goldstein H, Poole C. Safko J. *Classical mechanics*. USA: Addison-Wesley; 2002.
31. Shvetsov-Shilovski NI, Goreslavski SP, Popruzhenko SV, Becker W. Capture into Rydberg states and momentum distributions of ionized electrons. *Laser Phys*. 2009;19(8):1550–1558.
32. Shvetsov-Shilovski NI, Dimitrovski D, Madsen LB. Ionization in elliptically polarized pulses: Multielectron polarization effects and asymmetry of photoelectron momentum distributions. *Phys Rev A*. 2012;85(2):Article 023428.
33. Pfeiffer AN, Cirelli C, Smolarski M, Dimitrovski D, Abu-samha M, Madsen LB, Keller U. Attoclock reveals natural coordinates of the laser-induced tunnelling current flow in atoms. *Nat Phys*. 2012;8(1):76–80.
34. Bray AW, Eckart S, Kheifets AS. Keldysh-Rutherford model for the attoclock. *Phys Rev Lett*. 2018;121(12):123201.
35. Tulsky VA, Krebs B, Tiggesbumker J, Bauer D. Revealing laser-coherent electron features using phase-of-the-phase spectroscopy. *J Phys B At Mol Phys*. 2020;53(7):Article 074001.
36. Becker W, Goreslavski SP, Milošević DB, Paulus GG. The plateau in above-threshold ionization: The keystone of rescattering physics. *J Phys B At Mol Phys*. 2018;51(16):Article 162002.
37. Li M, Geng J-W, Han M, Liu M-M, Peng L-Y, Gong Q, Liu Y. Subcycle nonadiabatic strong-field tunneling ionization. *Phys Rev A*. 2016;93(1):Article 013402.
38. Li M, Liu M-M, Geng J-W, Han M, Sun X, Shao Y, Deng Y, Wu C, Peng L-Y, Gong Q, et al. Experimental verification of the nonadiabatic effect in strong-field ionization with elliptical polarization. *Phys Rev A*. 2017;95(5):Article 053425.
39. Trabert D, Anders N, Brennecke S, Schöffler MS, Jahnke T, Schmidt LPH, Kunitski M, Lein M, Dörner R, Eckart S. Nonadiabatic strong field ionization of atomic hydrogen. *Phys Rev Lett*. 2021;127(27):273201.
40. Liu K, Luo S, Li M, Li Y, Feng Y, Du B, Zhou Y, Lu P, Barth I. Detecting and characterizing the Nonadiabaticity of laser-induced quantum tunneling. *Phys Rev Lett*. 2019;122(5): Article 053202.